Preprint Title	Radiative Magnetohydrodynamics Casson Nanofluid Flow and Heat and Mass Transfer past on Nonlinear Stretching Surface
Authors	Gurrala Thirupathi, Kamatam Govardhan and Ganji Narender
Publication Date	23 Sep 2021
Article Type	Full Research Paper
ORCID® iDs	Gurrala Thirupathi - https://orcid.org/0000-0002-2269-0669; Kamatam Govardhan - https://orcid.org/0000-0003-0816-618X; Ganji Narender - https://orcid.org/0000-0003-1537-3793

Radiative Magnetohydrodynamics Casson Nanofluid Flow and Heat and Mass Transfer past on Nonlinear Stretching Surface

Gurrala Thirupathi[1], Kamatam Govardhan[2] and Ganji Narender[3*]

[1]Department of Mathematics, Rajiv Gandhi University of Knowledge Technologies, Basar, Nirmal, Telangana State, India.
[2]Department of Mathematics, GITAM University, Hyderabad, Telangana State, India.
[3]Department of Humanities & Sciences (Mathematics), CVR College of Engineering, Hyderabad, Telangana State, India.
*Corresponding author Email: gnriimc@gmail.com

Abstract
The magnetohydrodynamics (MHD) stagnation point Casson nanofluid flow towards stretching surface with velocity slip and convective boundary condition has been investigated in this article. Effects of thermal radiation, viscous dissipation, heat source and chemical reaction have also been incorporated. Using appropriate similarity transformation Partial Differential Equations (PDEs) are converted into Ordinary Differential Equations （ODEs) and shooting technique along with Adams–Moulton method of order four has been used to obtain the numerical results. Different physical parameters effects on velocity, temperature and concentration of nanofluid flow have been presented graphically and discussed in detail. Numerical values of the skin friction coefficient, Nusselt number and Sherwood number are also and discussed.

Key words: Casson Nanofluid, MHD, Thermal radiation, Chemical reaction, Viscous dissipation.

1. Introduction

Fluid is a phase of matter that deforms or flows under an applied external force. Fluid exists in the form of liquids, gases or plasma [1]. It is a substance with vanishing shear modulus or, in more simple words, substance which cannot resist any applied shear force. Fluid is the basic need of everyday life and because of its importance in many natural processes, scientists in different part of world are trying to explore various facts regarding the flow of fluid. Fluid dynamics is the sub-branch of fluid mechanics in which we study the fluid flow, also by analyzing the cause of flow. And how forces influence the fluid flow. It provides methods for understanding the evolutions of stars, ocean, current, tectonics plate, as well as the blood circulation [2]. Few important applications of fluid flows include wind turbines, oil pipelines, rocket engine and air-conditioning systems [3]. Archimedes was the first mathematician who formulated the Archimedes principle about the static of fluid and is considered to be the basics of fluid mechanics. The proper study of fluid mechanics start from early fifteen centuries. Fluid can be further classified into Newtonian or non-Newtonian fluid, depending on the relationship between two physical quantities i.e., stress and strain.

The mixture of nanoparticles with dimension less than 100nm and the conventional low thermal conductivity fluid is known as nanofluid. The word nanofluid was first introduced by Choi [4] that presented a new class of fluid. The thermal conductivity of nanofluid can be increased by using nanoparticle of gold, copper, silver etc., into the base fluid. The factor that lead to an increase in the thermal conductivity of nanofluids was studied by Buongiorno [5]. He observed that, both thermophoresis effect and the Brownian motion causes a change in thermal conductivity of the fluid. Naramgari and Soluchana [6] analyzed the effect of thermal radiation on MHD nanofluid over a stretching surface. Abolbashari et al. [7] investigated the transfer of energy and heat in the steady laminar Casson nanofluid flow using both slip velocity and surface boundary condition. Ghadikolaei et al. [8] investigated the influence of different physical parameters such as chemical reaction, thermal radiation, suction, Joule heating, heat generation and absorption in the MHD flow of Casson nanofluid using a porous non-linear sheet.

Magnetohydrodynamics is that branch of mechanics which we deals with the study of conduction fluid flow in the presence of an external magnetic field. It has wide range of applications in various fields of science such as, metallurgical science, mental working process, aerodynamics, fluid dynamics, and many others engineering disciplines for example, ceramic and biomedical engineering etc. [9]. The 2D mixed convection MHD boundary layer stagnation point flow in the existence of thermal radiation using a vertical plate which was filled with nanofluid has been demonstrated by Eftekhari and Moradi [10]. Kumar et al. [11] analyzed the impact of the transfer of heat in MHD Casson nanofluid using nonlinear surface. Aman et al. [12] investigated the flow of 2D incompressible viscous fluid using a shrinking surface in the existence of an external magnetic field.

Stagnation point always exist on the flow field surface such that close to this point the fluid come to at rest. There for, the Stagnation point can be defined as, the point in the flow field where the fluid velocity become zero. The study of the flow of nanofluid close to the stagnation point has many practical applications, some of them are listed as, cooling of electronic devices by fan, solar receiver, the cooling of nuclear reactor at the time of emergency shutdown, and several hydrodynamic processes [13]. Due to these important applications of stagnation point flow has attracted a great attention of scientific community. Hiemenz [14] was the first mathematician who first time proposed the 2D stagnation point flow. Eckert [15] got the accurate solution by extending Hiemenz problem by adding the energy equation. Mahapatra and Gupta [16], In view of that Ishak et al. [17], and Hayat et al. [18] investigated the impact of the transfer of heat on stagnation point over a porous plate.

Non-Newtonian fluid has wide range of application such as oil recovery, filtration, polymer engineering, ceramics production and petroleum production. There is exists a sub-class of non-Newtonian fluids called Casson fluid. This fluid has large viscosity which tends to infinity at zero rate of shear i.e., if the magnitude of shear stress is much weaker than the magnitude of applied stress it behaves like a solid. On the other hand, if shear stress become greater than the yield stress the fluid start flowing. Casson [19] first time developed the Casson model for various suspension of cylindrical particles. Soup, fruit juice, jelly, honey and tomatoes sauce are general example of Casson fluid. Benazir et al. [20] have analyzed the unsteady MHD Casson fluid flow over a at plate and vertical

cone over porous medium along with double dispersion effects. The laminar convective boundary layer non-Newtonian Casson fluid flow thermally fixed over a stretching sheet have been analyzed by Animasaun et al. [21] Afikuzzaman et al. [22] have investigated the unsteady flow of MHD fluid with hall current through parallel plates and considering the magnetic field perpendicular to the plates. The heat transfer with MHD Casson fluid flow towards a linear stretching sheet with temperature distribution over the sheet has been analyzed by Govardhan et al. [23]. In this article, we provide a detail review of Ibrahim et al. [24] study and the study is extended by considering various other effects such as Soret effect, Dufour effect and inclined magnetic field.

2. Problem Formulation

We have considered a 2D steady incompressible MHD stagnation point flow of a Casson nanofluid over a stretching sheet. The sheet is placed in the plane $y=0$, such that $y-$ axis is normal to the sheet. The flow of nanofluid is constrained to the surface $y>0$, the origin is kept fixed while the sheet is stretching with velocity $u=u_w(x)=ax^n$ with $n\geq 0$ and $u_\infty = bx^n$ is the free stream velocity where a and b are two positive constants. The slip velocity at the surface is taken as $U_{slip}=\left(\mu B+\frac{p_y}{\sqrt{2\pi_c}}\right)\frac{\partial u}{\partial y}$. Where π_c is the critical value of this product based on the non-Newtonian model, μB is the plastic dynamic viscosity and p_y is the yield stress. The magnetic field $B(x)=B_0 x^{\frac{n-1}{2}}$ is applied normal to the sheet where B_0 is a constant. It is also assumed that the magnetic Reynolds number is small, and the induced magnetic field is negligible. A convective heating process is used to regulate the sheet temperature T_f. The nanoparticles concentration is C_w which is assumed to be constant. For y goes to infinity, the concentration and temperature of nanofluid is represented by C_∞ and T_∞ respectively.

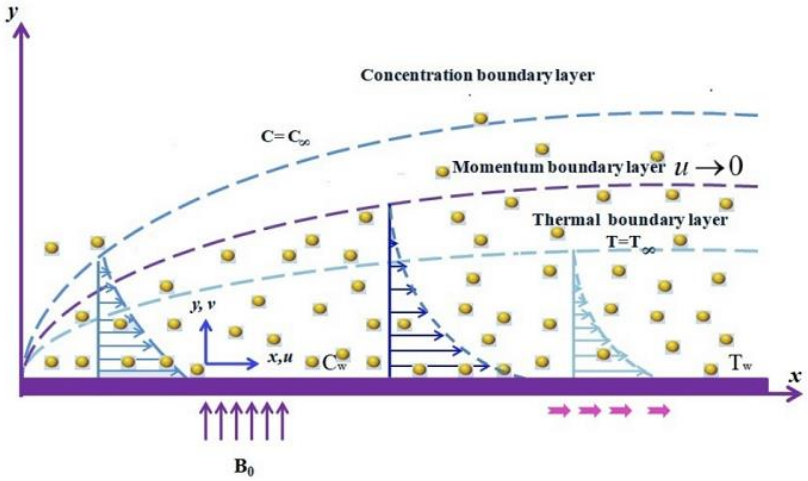

Figure 1: Flow model geometry.

The boundary layer equations in the light of above assumptions are

Continuity equation

Physical principal: Mass is conserved

$$\frac{\partial u}{\partial x}+\frac{\partial v}{\partial y}=0, \tag{1}$$

Momentum equation

Physical principle: F = ma

$$u\frac{\partial u}{\partial x}+v\frac{\partial u}{\partial y}=\nu\left(1+\frac{1}{\beta}\right)\frac{\partial^2 u}{\partial y^2}+U_\infty\frac{\partial U_\infty}{\partial x}+\frac{\sigma B^2}{\rho_f}\left(U_\infty-u\right), \tag{2}$$

Energy equation

Physical principle: Energy is conserved

$$\left.\begin{aligned} u\frac{\partial T}{\partial x}+v\frac{\partial T}{\partial y}=\alpha\left(\frac{\partial^2 T}{\partial y^2}\right)+\frac{\nu}{C_p}\left(1+\frac{1}{\beta}\right)\left(\frac{\partial u}{\partial y}\right)^2+\frac{1}{\left(\rho c\right)_f}\frac{Q_0}{\left(T-T_\infty\right)}-\frac{1}{\left(\rho c\right)_f}\frac{\partial q_r}{\partial y} \\ +\frac{\left(\rho c\right)_p}{\left(\rho c\right)_f}\left[D_B\frac{\partial C}{\partial y}\frac{\partial T}{\partial y}+\frac{D_T}{T_\infty}\left(\frac{\partial T}{\partial y}\right)^2\right], \end{aligned}\right\} \tag{3}$$

Mass transfer equation

$$u\frac{\partial C}{\partial x}+v\frac{\partial C}{\partial y}=D_B\left(\frac{\partial^2 C}{\partial y^2}\right)+\frac{D_T}{T_\infty}\left(\frac{\partial^2 T}{\partial y^2}\right)-k_0\left(C-C_\infty\right), \tag{4}$$

The corresponding boundary conditions are:

$$\left.\begin{aligned} &u=U_w+U_{slip}=ax^n+\left[\mu_B+\frac{P_y}{\sqrt{2\pi_c}}\right]\frac{\partial u}{\partial y},\quad v=v_w, \\ &-k\left(\frac{\partial T}{\partial y}\right)=h_f\left[T_f-T\right],\ \ C=C_w \end{aligned}\right\} at\ \ y=0, \\ u\to U_\infty=bx^n,\quad v\to 0,\quad T\to T_\infty,\quad C\to C_\infty\quad as\quad y\to\infty. \tag{5}$$

In the above equations, ν stands for kinematic viscosity, ρ_f for fluid density, α represent thermal diffusivity, C_p represents specific heat at constant pressure, k_0 denotes chemical reaction coefficient and $\left(\rho c\right)_f$ represents heat capacity, D_B represents Brownian diffusion coefficient, Q_0 shows volumetric heat generation, D_T thermophoresis diffusion coefficient, U_∞ represents free stream velocity n indicates nonlinear stretching parameter, σ shows the electrical conductivity, β represents the Casson fluid parameter, sheet

temperature can be represented by T_w and T represents nanofluid temperature respectively. C is nanoparticles concentration, C_p shows the free stream concentration and h_f denotes the coefficient of heat transfer.

3. Similarity Transformation

The following transformation [24] has been used to get ODEs from PDEs

$$\left.\begin{aligned} &u = a\,x^n f'(\xi),\quad v = -\sqrt{\frac{a\nu(n+1)}{2}}\,x^{\frac{n-1}{2}}\left(f(\xi)+\frac{n-1}{n+1}\xi f'(\xi)\right),\\ &\xi == y\sqrt{\frac{a(n+1)}{2\nu}}\,x^{\frac{n-1}{2}},\quad \psi(x,y) = \sqrt{\frac{2a\nu}{(n+1)}}\,x^{\frac{n+1}{2}} f(\xi),\\ &\theta(\xi) = \frac{T-T_\infty}{T_f-T_\infty}\qquad \phi(\xi) = \frac{C-C_\infty}{C_w-C_\infty}. \end{aligned}\right\} \tag{6}$$

The following assumptions are made for the calculation of velocity components along x and y direction as

$$u = \frac{\partial\psi}{\partial y},\qquad v = -\frac{\partial\psi}{\partial x}. \tag{7}$$

The non-dimensional form of the Eqs. (2), (3) and (4) are:

$$\left(1+\frac{1}{\beta}\right)f''' + ff'' - \frac{2n}{n+1}\left(\left(f'\right)^2 - A^2\right) + M\left(A - f'\right) = 0, \tag{8}$$

$$\left(1+\frac{4R}{3}\right)\theta'' + \Pr\, f\theta' + + \Pr\left(Nb\theta'\phi' + Nt\left(\theta'\right)^2\right) + \left(1+\frac{1}{\beta}\right)Ec\Pr\left(f''\right)^2 + \Pr Q\theta = 0,$$

(9)

$$\phi'' + Le\ f\phi' + \frac{Nt}{Nb}\theta'' - Le\,\gamma\,\phi = 0. \tag{10}$$

The corresponding boundary condition becomes

$$\left.\begin{aligned} &f(\xi) = 0,\ f'(\xi) = 1+\delta\left(1+\frac{1}{\beta}\right)f''(\xi),\\ &\theta'(\xi) = -Bi\left(1-\theta(\xi)\right),\quad \phi(\xi) = 1\ , \end{aligned}\right\}\ at\quad \xi = 0,$$

$$f'(\xi)\to A,\quad \theta(\xi)\to 0,\quad \phi(\xi)\to 0,\ as\quad \xi\to\infty.$$

(11)

In the above Eqs. (8)-(11) R represents the radiation parameter, $\Pr$ stands for Prandtl number, Bi the Biot number, Ec for Eckert number, Nb represents Brownian motion parameter, Nt the thermophoresis parameter, Q represents the heat generation, Le stands for the Lewis number, A denotes velocity ratio number and S is the suction parameter, these parameter are formulated as:

$$\left.\begin{aligned} &A=\frac{b}{a}, M=\frac{2\sigma B_0^2}{a\rho_f\left(n+1\right)}, Nb=\frac{\left(\rho c\right)_p D_{\mathrm{B}}\left(C_w-C_\infty\right)}{\nu\left(\rho c\right)_f}, R=\frac{4\sigma^* T_\infty^3}{k^* k}, Le=\frac{\nu}{D_{\mathrm{B}}},\\ &Q=\frac{2xQ_0}{a\rho_f\left(n+1\right)U_w}, \quad Ec=\frac{U_w^2}{C_p\left(T_f-T_\infty\right)}, \quad Nt=\frac{\left(\rho c\right)_p D_T\left(T_f-T_\infty\right)}{\nu\left(\rho c\right)_f T_\infty},\\ &\mathrm{Pr}=\frac{\nu}{\alpha}, \quad Bi=\frac{h_f}{k}\sqrt{\frac{2\nu}{a\left(n+1\right)}}\frac{1}{x^{\frac{n-1}{2}}},. \end{aligned}\right\} \tag{12}$$

4. Physical Quantities of Interest

Mathematical form of skin coefficient friction is

$$C_{fx}=\frac{\tau_w}{\rho U_w^2}, \tag{13}$$

Mathematical form of Nusselt number is

$$Nu_x=\frac{xq_w}{k\left(T_f-T_\infty\right)}, \tag{14}$$

And the Sherwood number is

$$Sh_x=\frac{xq_m}{D_B\left(C_w-C_\infty\right)}, \tag{15}$$

In the above equations q_w represents the heat flux, τ_w the shear stress, and q_m denotes the mass flux which are defined as

$$\tau_w=\mu\left(1+\frac{1}{\beta}\right)\left(\frac{\partial u}{\partial y}\right)_{y=0}, q_w=\left(-\left(k+\frac{16\sigma^* T_\infty^3}{3k^*}\right)\left(\frac{\partial T}{\partial y}\right)\right)_{y=0}, q_m=-D_B\left(\frac{\partial C}{\partial y}\right)_{y=0}. \tag{16}$$

We obtained the following dimensionless form for Nusselt number Sherwood number and skin friction coefficient:

$$\mathrm{Re}_x^{0.5} C_f\sqrt{\frac{2}{n+1}}=\left(1+\frac{1}{\beta}\right)f^{''}\left(0\right), \ \mathrm{Re}_x^{-0.5} Nu_x\sqrt{\frac{2}{n+1}}=-\left(1+\frac{4}{3}R\right)\theta^{'}\left(0\right),$$

$$\mathrm{Re}_x^{-0.5} Sh_x\sqrt{\frac{n+1}{2}}=-\phi^{'}\left(0\right).$$

The Reynolds number can be defined as $\mathrm{Re}_x=\frac{U_w x}{\nu}$.

5. Solution Methodology

The system of nonlinear ODEs (8)-(10) along with boundary condition (10) are converted into first order ODEs. The first order system of ODEs with appropriate boundary condition are solved by using shooting method. We adopt the following procedure:

$$f''' = \frac{-ff'' + \frac{2n}{n+1}\left(\left(f'\right)^2 - A^2\right) - M\left(A - f'\right)}{\left(1+\frac{1}{\beta}\right)}, \tag{17}$$

$$\theta'' = \frac{-\Pr\left[f\theta' + Nb\theta'\phi' + Nt\left(\theta'\right)^2 + \left(1+\frac{1}{\beta}\right)Ec\left(f''\right)^2 + Q\theta\right]}{\left(1+\frac{4R}{3}\right)}, \tag{18}$$

$$\phi'' = -Le\ f\phi' - \frac{Nt}{Nb}\theta'' + Le\gamma\phi. \tag{19}$$

Since Eq. (17) is a function of f and its derivatives, which can be solved individually by shooting method. The solution of Eq. (17) can be used in Eq. (18) and Eq. (19) as a recognize input. We have notice two initial conditions given at $\eta = 0$ in the above third order ODE, Eq. (17) give the unknown condition $f''(0)$ which is represented by P. We have introduced the following symbols for further simplification.

$$f = y_1,\ f' = y_2,\ f'' = y_3, \frac{\partial f}{\partial P} = y_4,\ \frac{\partial f'}{\partial P} = y_5, \frac{\partial f''}{\partial P} = y_6.$$

The above system of ODEs and the corresponding initial condition can be written as

$$\left.\begin{aligned}
y_1' &= y_2, & y_1(0) &= S,\\
y_2' &= y_3, & y_2(0) &= 1+\delta\left(1+\frac{1}{\beta}\right)P,\\
y_3^1 &= \frac{1}{\left(1+\frac{1}{\beta}\right)}\left[\frac{2n}{n+1}\left(y_2^2 - A^2\right) - y_1y_3 - M\left(A - y_2\right)\right], & y_3(0) &= P,\\
y_4' &= y_5, & y_4(0) &= 0,\\
y_5^1 &= y_6, & y_5(0) &= \delta\left(1+\frac{1}{\beta}\right),\\
y_6' &= \frac{1}{\left(1+\frac{1}{\beta}\right)}\left[-y_1y_6 - y_4y_3 + \frac{2n}{n+1}\left(2y_2y_5\right) + My_5\right], & y_6(0) &= 1.
\end{aligned}\right\} \tag{20}$$

For the solution of above initial value problem, we use Adams Moulton Method of order four. For finding the initial condition we take $P = P^{(0)}$. For calculating the root, we used Newton method which is given by the following iteration

$$P^{(n+1)} = P^{(n)} * -\left(\frac{y_2\left(\xi_\infty, P^{(n)} - A\right)}{y_5\left(\xi_\infty, P^{(n)}\right)}\right). \tag{21}$$

The approximate solution of Eq. (17) can be obtained by converting the unbounded domain $[0,\infty)$ into bounded domain $[0,\xi_{\max}]$, where $\xi_{\max}$ is chosen such that no considerable changes are obtained going beyond. The execution of the Newton's method can be presented in the following algorithmic form:

Step-1: Choose an initial guess $r = r_0$ in the equation (8) and solve it by the Adams-Moulton method.

Step-2: If for a very small positive number ε,

$\left|h_2\left(r^k\right)_{\eta=\eta_\infty} - A\right| > \varepsilon$, for $k = 0,1,2,.....$

then go to Step-3, otherwise the solution is there.

Step-3: Compute the next value of the missing initial condition r^{k+1}; $k = 0,1,2,.....$ by using the Newton's scheme given by (21).

Step-4: Repeat Step-1 with $r = r^{k+1}$.

In order to apply numerical method for the solution of Eqs. (18) and Eq. (19), we denote the missing initial condition $\theta(0)$ and $\phi(0)$ by q and r, respectively and different notations have been used which are given below

$$\theta = Z_1, \theta' = Z_2, \phi = Z_3, \phi' = Z_4, \frac{\partial\theta}{\partial q} = Z_5, \frac{\partial\theta'}{\partial q} = Z_6, \frac{\partial\phi}{\partial q} = Z_7, \frac{\partial\phi'}{\partial q} = Z_8,$$

$$\frac{\partial\theta}{\partial r} = Z_9, \frac{\partial\theta'}{\partial r} = Z_{10}, \frac{\partial\phi}{\partial r} = Z_{11}, \frac{\partial\phi'}{\partial r} = Z_{12}$$

Using these notations, we get a system of first order ODEs which are given below

$$Z_1' = Z_2, \qquad Z_1(0) = q,$$

$$Z_2' = \frac{-\Pr}{\left(1+\frac{4}{3}R\right)}\left[y_1 Z_2 + Nb\, Z_2\, Z_4 + \left(1+\frac{1}{\beta}\right)Ecy_3^2 + Nt\, Z_2^2 + Q\, Z_1\right], \qquad Z_2(0) = -Bi(1-q),$$

$$Z_3' = Z_4, \qquad Z_3(0) = 1,$$

$$Z_4' = -Le\, y_1 Z_4 + \frac{3\,Nt\,\Pr}{Nb(3+4R)}\left[y_1 Z_2 + Nb\, Z_2\, Z_4 + \left(1+\frac{1}{\beta}\right)Ecy_3^2 + Nt\, Z_2^2 + Q\, Z_1\right] + Le\,\gamma\, Z_3, \qquad Z_4(0) = r,$$

$$Z_5' = Z_6, \qquad Z_5(0) = 1,$$

$$Z_6' = \frac{-\Pr}{\left(1+\frac{4}{3}R\right)}\left[y_1 Z_6 + Nb\left(Z_6\, Z_4 + Z_2\, Z_8\right) + 2\,Nt\, Z_2\, Z_6 + Q\, Z_5\right], \qquad Z_6(0) = Bi,$$

$$Z_7' = Z_8, \qquad Z_7(0) = 0,$$

$$Z_8' = -Le\, y_1 Z_8 + \frac{3\,Nt\,\Pr}{Nb(3+4R)}\left[y_1 Z_6 + Nb\left(Z_6\, Z_4 + Z_2\, Z_8\right) + 2\,Nt\, Z_2\, Z_6 + Q\, Z_5\right] + Le\,\gamma\, Z_7, \qquad Z_8(0) = 0,$$

$$Z_9' = Z_{10}, \qquad Z_9(0) = 0,$$

$$Z_{10}' = \frac{-\Pr}{\left(1+\frac{4}{3}R\right)}\left[y_1 Z_{10} + Nb\left(Z_{10}Z_4 + Z_2 Z_{12}\right) + 2Nt\, Z_2 Z_{10} + Q Z_9\right], \qquad Z_{10}(0) = 0,$$

$$Z_{11}' = Z_{12}, \qquad Z_{11}(0) = 0,$$

$$Z_{12}' = -Le\, y_1 Z_{12} + \frac{3Nt\Pr}{Nb\left(3+4R\right)}\left[y_1 Z_{10} + Nb\left(Z_{10}Z_4 + Z_2 Z_{12}\right) + 2Nt\, Z_2 Z_{10} + Q Z_9\right] + Le\,\gamma Z_{11}, \qquad Z_{12}(0) = 1.$$

In order to solve the above initial value problem, we used Adams Moulton method and the missing conditions are chosen such that

$\left(Z_1(q,r)\right)_{\xi=\xi_\infty} = 0, \qquad \left(Z_3(q,r)\right)_{\xi=\xi_\infty} = 0.$

The above set of equations can be solved by using Newtons method with following iterative formula:

$$\begin{bmatrix} q^{(n+1)} \\ r^{(n+1)} \end{bmatrix} = \begin{bmatrix} q^{(n)} \\ r^{(n)} \end{bmatrix} - \begin{bmatrix} \frac{\partial Z_1(q,r)}{\partial q} & \frac{\partial Z_1(q,r)}{\partial r} \\ \frac{\partial Z_3(q,r)}{\partial q} & \frac{\partial Z_3(q,r)}{\partial r} \end{bmatrix}^{-1} \begin{bmatrix} Z_1 \\ Z \end{bmatrix}_{\left(q^{(n)}, r^{(n)}, \xi_\varphi\right)}$$

$$\Rightarrow \begin{bmatrix} q^{(n+1)} \\ r^{(n+1)} \end{bmatrix} = \begin{bmatrix} q^{(n)} \\ r^{(n)} \end{bmatrix} - \begin{bmatrix} Z_5 & Z_9 \\ Z_7 & Z_{11} \end{bmatrix}^{-1} \begin{bmatrix} Z_1 \\ Z \end{bmatrix}_{\left(q^{(n)}, r^{(n)}, \xi_\varphi\right)} \tag{22}$$

The following steps are involved for the accomplishment of the shooting method.

(i) Choice of the guesses $q = q_0$ and $r = r_0$.

(ii) Choice of a positive small number δ.
If $\max\left\{\left|Z_1(\eta_\infty - 0)\right|, \left|Z_3(\eta_\infty - 0)\right|\right\} < \delta$, stop the process otherwise go to (iii).

(iii) Compute q^{k+1} and r^{k+1}; $k = 0,1,2,3,4.....$by using (22).

(iv) Repeat (i) and (ii). In a similar manner, the ODEs (9-10) along with the associated BCs can be solved by considering f as a known function.

The stopping criteria for the shooting method is set as: $\max\left\{\left|Z_1(\xi_\infty)\right|, \left|Z_3(\xi_\infty)\right|\right\} < \in$,

where $\in$ is a small positive number. From now onward $\in$ has been taken as 10^{-8} whereas ξ_∞ is set as 7.

6. Results and Discussion

The numerical results of the equations in the previous sections are discussed in this section by using the graphs and tables. The numerical computations are done for the influence of different important parameters such as, thermal radiation R, nonlinear parameter $\eth$, Casson fluid parameter β, thermophoresis parameter Nt, magnetic parameter M, velocity parameter, skin friction coefficient, Brownian parameter, Sherwood and Nusselt number. These physical parameters have a direct effect on concentration, temperature and velocity distribution.

Skin-Friction Coefficient, Nusselt Number and Sherwood Numbers

Table 1 and 2 describes the computed numerical results of Nusselt's number, Sherwood number and skin friction coefficient using different physical parameters given in the table. The skin friction coefficient is $-\left(1+\frac{1}{\beta}\right)f''(0)$, the Nusselt number is $-\left(1+\frac{4}{3}R\right)\theta'(0)$, and the Sherwood number is $-\phi'(0)$. The values of skin friction coefficient, Nusselt number and Sherwood number changes by changing the physical parameters. As given in the table, the skin friction coefficient gradually depressed by taking large values of slip parameter, Brownian parameter, chemical reaction parameter, thermophoresis parameter and Biot number, however for thermal radiation and Ekert number no change has been observed in the skin friction coefficient. The table clearly shows gradual decrease in Nusselt and Sherwood number by enhancing the numerical values of various physical parameters.

Table 1: Computed numerical data of skin friction coefficient, for $M = 0.5, \beta = 1.0, S = 1.0, A = 0.2, n = 2.0.$

δ	R	Nb	Nt	Ec	Q	Bi	γ	$-\left(1+\frac{1}{\beta}\right)f''(0)$	Present
0.1	0.1	0.2	0.2	0.1	0.1	0.5	0.2	1.61508	1.615085
0.5								0.86635	0.8663513
1.0								0.55611	0.5561473

Table 2: Computed numerical data of Nusselt and Sherwood number for $M = 0.5, \beta = 1.0, S = 1.0, A = 0.2, n = 2.0.$

δ	R	Nb	Nt	Ec	Q	Bi	γ	$-\left(1+\frac{4}{3}R\right)\theta'(0)$	Present	$\phi'(0)$	Present
0.1	0.1	0.2	0.2	0.1	0.1	0.5	0.2	0.31881	0.31851990	0.78212	0.78184500
0.5								0.31584	0.31572310	0.73225	0.73172220
1.0								0.29743	0.31209230	0.69361	0.71006290
	0.5							0.47534	0.40664310	0.85635	0.82238190
	0.7							0.54226	0.44421670	0.86696	0.83734510
		0.5						0.52735	0.49954630	0.91883	0.89945870
		0.1						0.30714	0.32305150	0.75428	0.57684580
			0.3					0.49898	0.31734510	0.93392	0.68620830
			0.5					0.31618	0.31492500	0.75528	0.49861680
				0.5				0.37008	0.26913770	0.82365	0.83793130
				1.0				0.47926	0.20716610	0.94256	0.90818040
					-0.2			0.51145	0.34502760	0.92416	0.75364970
					0.0			0.35468	0.32873450	0.83659	0.77109130
						0.1		0.15916	0.09567917	0.94445	0.92249670
						2.0		0.52619	0.56139440	0.82931	0.62964730
							0.0	0.52985	0.31901520	0.72444	0.66415260
							0.5	0.52180	0.31798700	0.96569	0.92964540

Effect of Casson Parameter β

Figure 2 analyzes the impact of β on dimensional velocity profile. The velocity of the fluid decreases by increasing the numerical value of β. Physically, this means that fluid viscosity increases due to accelerating values of β which in turn decelerate the nanofluid velocity profile. Furthermore, the present phenomena convert to Newtonian fluid as β approaches to infinity. Figure 3 illustrates the relationship between energy profile and β. It is seen that the temperature distribution of the fluid increases by gradually increasing the value of β. Actually, by increasing value of β the thermal boundary thickness increase due to which the surface temperature increases. Figure 4 demonstrates the behavior of β on the concentration field. The nanoparticle volume fraction is observed to be increased for the higher estimation of β.

Effect of Magnetic Number M

Figure 5 shows the relationship between M on dimensionless velocity profile $f'(\eta)$, we see that the velocity profile of the fluid depressed continuously by accelerating the value of magnetic field. Generally, the increasing value of M creates the Lorentz force and the collision between the conducting molecules increase in the presence of this force due to which the temperature of the fluid increases and the velocity decreases at the boundary layer. Figure 6 illustrates the dependence of energy profile on magnetic parameter M. From the graph, we see that gradually enhancement of M causes an increase in the temperature. Physically, the greater magnetic number induces an opposing force normally known as the Lorentz force which significantly increase both boundary layer thickness and temperature profile of the nanofluid. Figure 7 analyzes the behavior of concentration distribution for ascending values of M. The graph shows that the fluid concentration distribution is enhanced with mounting values of M.

Effect of Eckert Number Ec

Figure 8 illustrates the impact of Ec on temperature profile of the fluid. The graph clearly shows that the temperature distribution is enhanced by mounting values of Ec. Actually, Ec can be written as a ratio of kinetic energy of the fluid particle and thermal energy. The increasing value of Ec means, we have increased the kinetic energy of the fluid particle, as a result the thermal boundary layer thickness is enhanced.

Effect of Thermophoresis Parameter Nt

Figure 9 investigates the dependence of temperature distribution on Nt. The plot shows that the temperature profile of the fluid is escalating with boosting values of Nt. Actually, reason of this behavior is that the nanoparticle at the hot boundary side have been moved towards the cold boundary side and the thermal boundary layer become thicker in the existence of Nt. Figure 10 depicts the visualization of Nt on the concentration distribution. It is noticed that by gradually increasing Nt the concentration distribution also increases. Generally, in the presence of Nt exert forces on each other, as a result particle move from hotter to colder region of the fluid and has been noticed an increment in the concentration distribution.

Effect of Biot Number Bi

Figures 11 and 12 are drawn to analyze the impact of Bi on both energy and concentration distribution of the fluid respectively. Physically, Bi can be written as a ratio of convection to conduction. The convection is taking place on the surface while the conduction is taking place inside the surface. Thus, the boosting value of Bi accelerates both temperature and concentration profile.

Effect of Velocity Slip Parameter δ

Figure 13 shows the relationship between slip parameter and dimensionless velocity distribution. The velocity is observed to be a reducing function of δ. It can be generalized as the fractional resistance between fluid particles and the flow surface increases as a result the velocity profile of the fluid decreases. Figure 14 shows that the energy profile is accelerated by gradually uprising the value of δ.

Effect of Radiation Parameter R

Figure 15 analyzes the impact of R on energy distribution. The gradually rising value of R enhances the energy distribution of the fluid. Actually, the heat energy exhausted from the fluid due to large value of R and as a result the energy distribution increased.

Effect of Prandtl Number $\Pr$

Figure 16 explores the impact of $\Pr$ on energy distribution. Since, the $\Pr$ can be written as a ratio of kinematic diffusivity to heat diffusivity. The gradually increasing value of $\Pr$ increase the fluid density and decreasing thermal diffusivity and as a result the energy distribution is enhanced.

Effect of Heat Generation/Absorption Coefficient Q

Figure 17 illustrates the relationship between Q and temperature profile of the fluid. The plot clearly shows a reduction in temperature distribution of the fluid for negative value of Q. In the same way heat generation occurs for the positive value of Q. Due to these behaviors the temperature of the fluid gradually increases.

Effect of Brownian Motion Parameter Nb

Figure 18 is drawn to illustrate the relationship between Nb and temperature distribution. The temperature distribution is enhanced with rising value of Nb. Physically, Nb is associated with movement of the fluid nanoparticles. The kinetic energy of the fluid particles increases with boosting values of Nb, due to which the temperature distribution of the fluid increases. Figure 19 is drawn to analyze the effect of Nb on concentration profile, which shows that the increasing value of Nb produce a reduction in concentration distribution.

Effect of Suction Parameter S

Figures 20-22 show the relationship between S and velocity, S and temperature and S and concentration profile respectively. From the graphs it is observed that increasing the numerical value of S a decrement in the velocity, temperature and concentration profile of the fluid occur.

Effect of Lewis Number *Le*

Figure 23 analyzed the relation between the Lewis number *Le* and concentration distribution. Concentration profile decreased for high value of *Le* and thus we have got a small molecular diffusivity. Generally, concentration profile is a decreasing function of Lewis number.

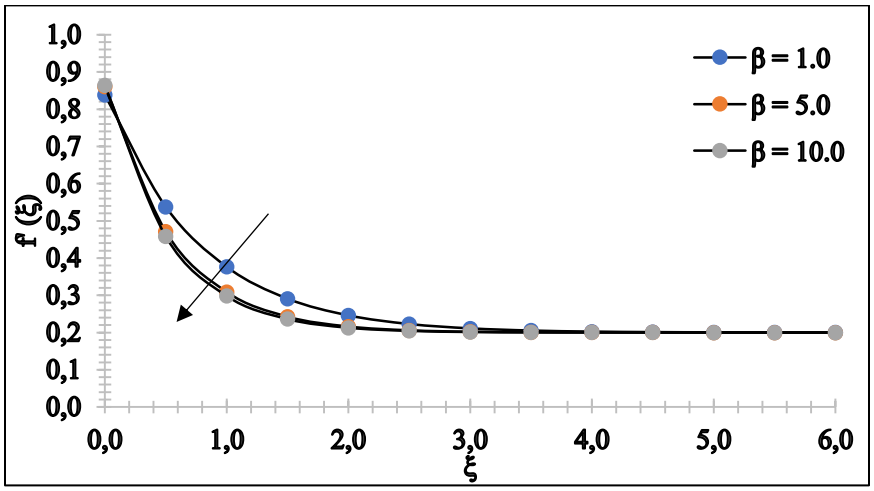

Figure 2: Influence of β on $f'(\xi)$.

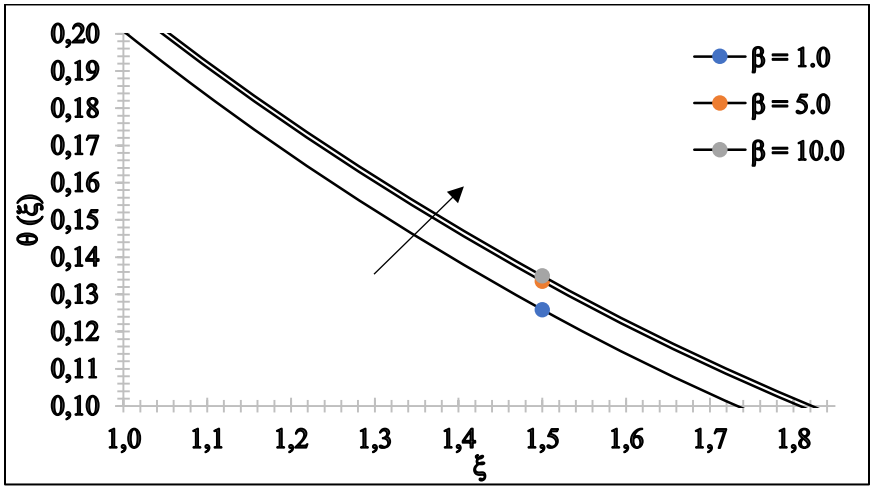

Figure 3: Influence of β on $\theta(\xi)$.

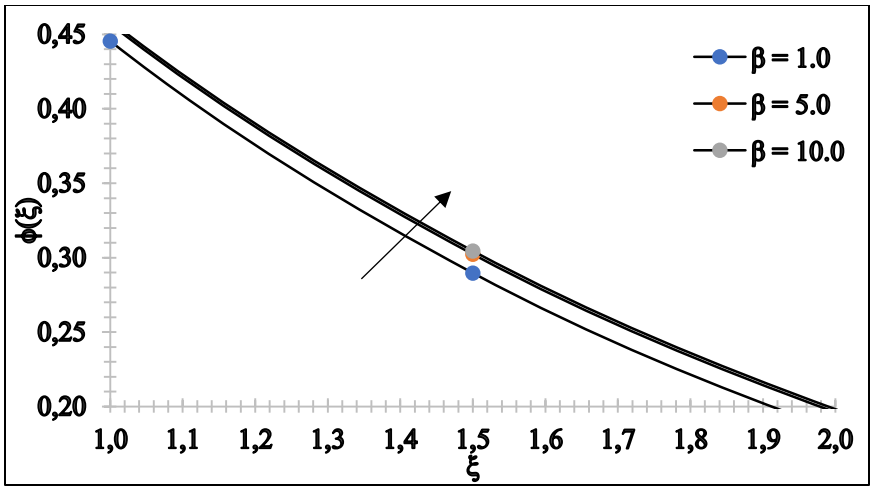

Figure 4: Influence of β on $\phi(\xi)$.

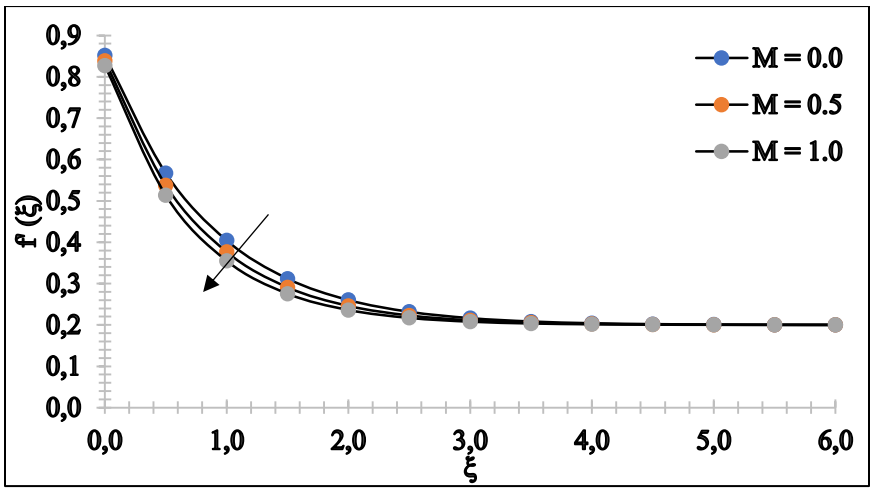

Figure 5: Influence of M on $f'(\xi)$.

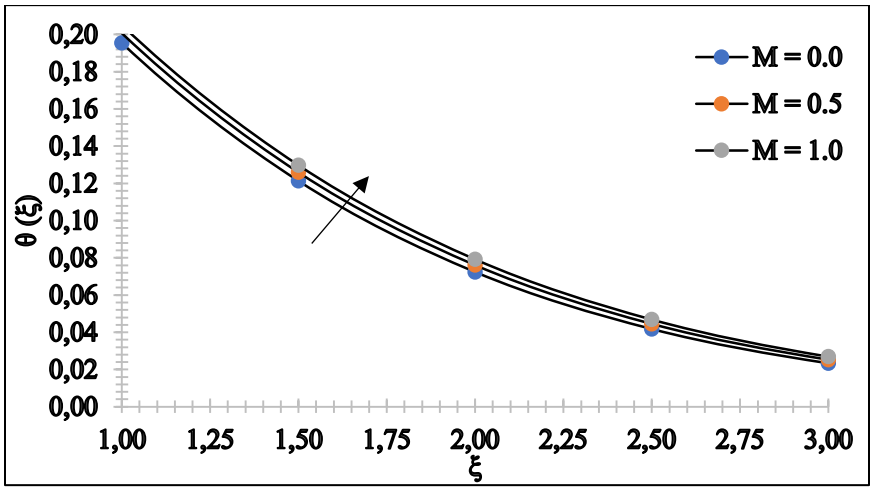

Figure 6: Influence of M on $\theta(\xi)$.

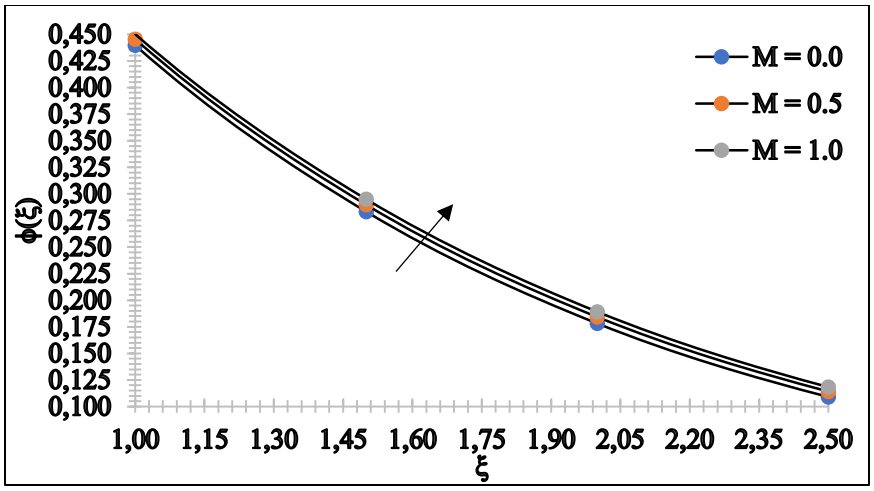

Figure 7: Influence of M on $\phi(\xi)$.

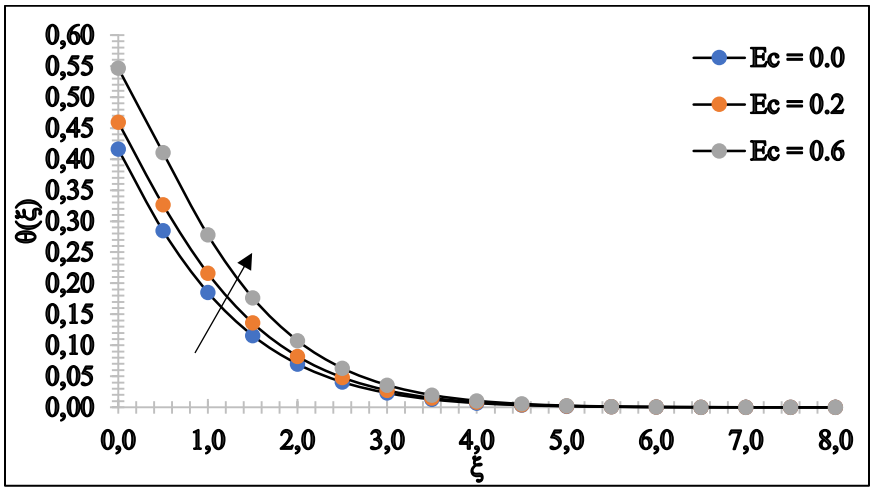

Figure 8: Influence of Ec on $\theta(\xi)$

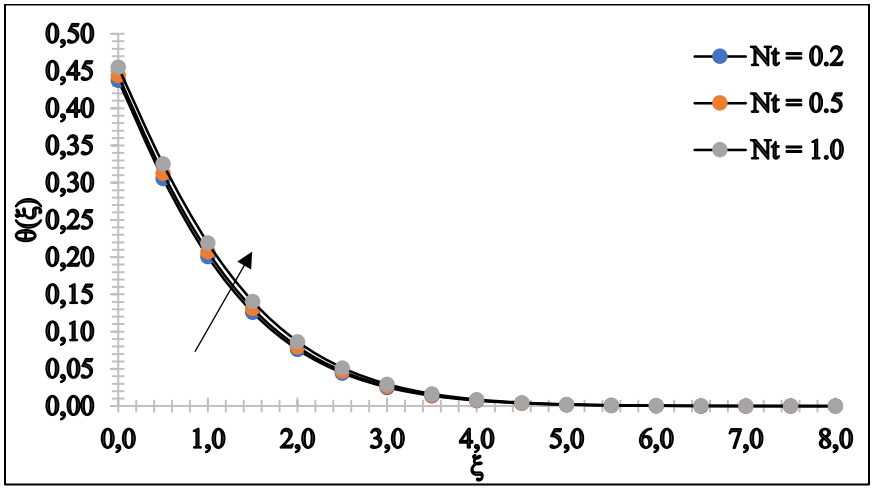

Figure 9: Influence of Nt on $\theta(\xi)$

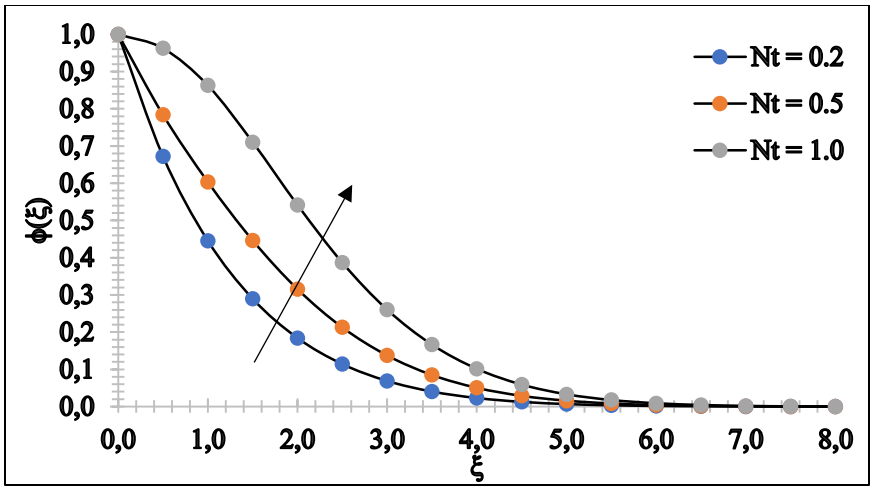

Figure 10: Influence of Nt on $\phi(\xi)$

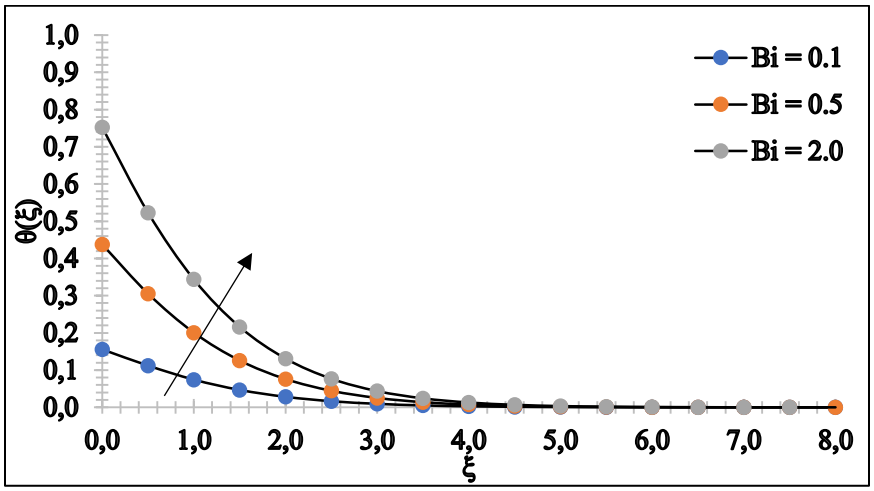

Figure 11: Influence of Bi on $\theta(\xi)$

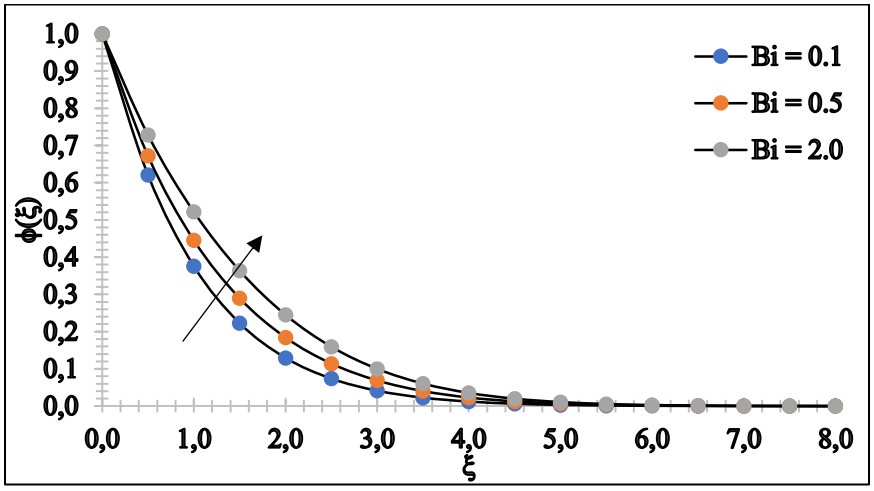

Figure 12: Influence of Bi on $\phi(\xi)$

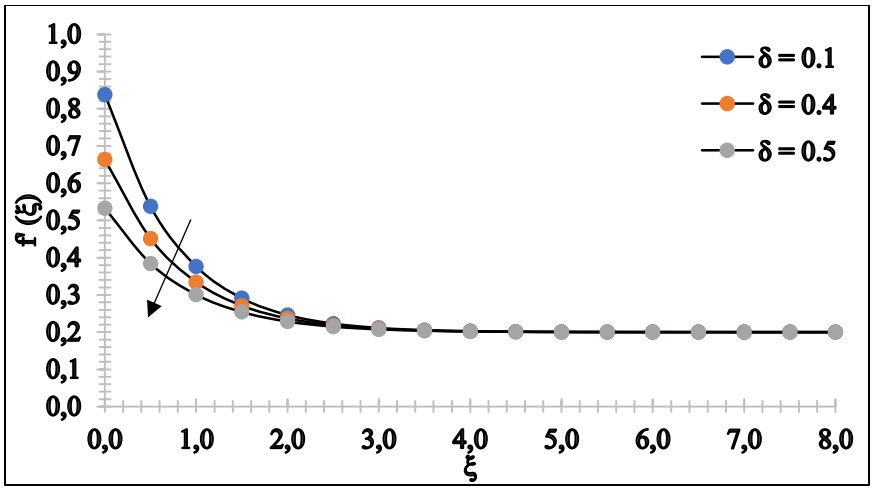

Figure 13: Influence of δ on $f'(\xi)$.

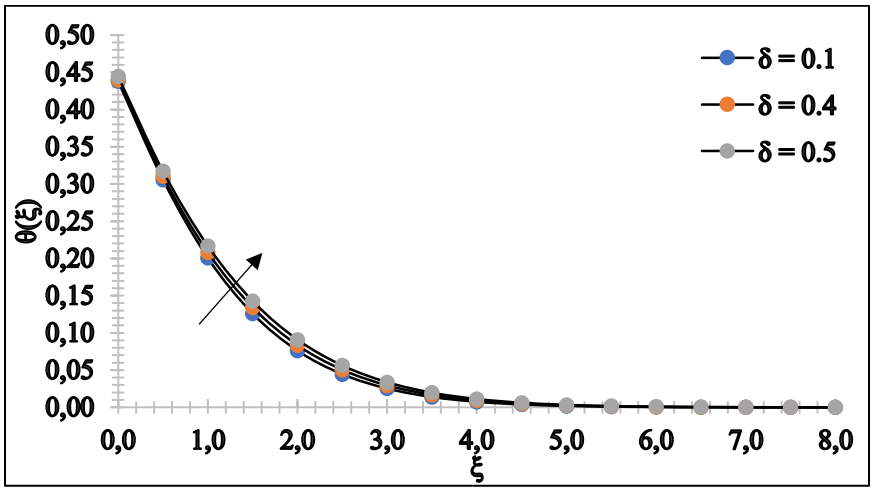

Figure 14: Influence of δ on $\theta(\xi)$.

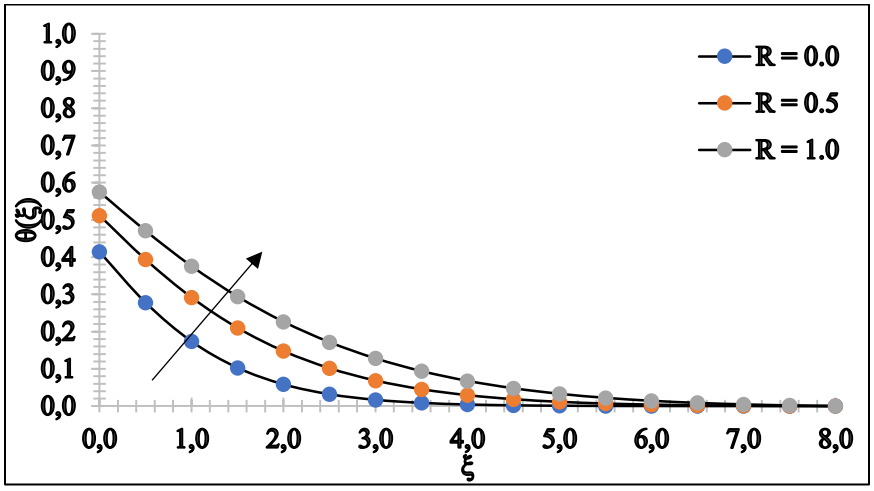

Figure 15: Influence of R on $\theta(\xi)$.

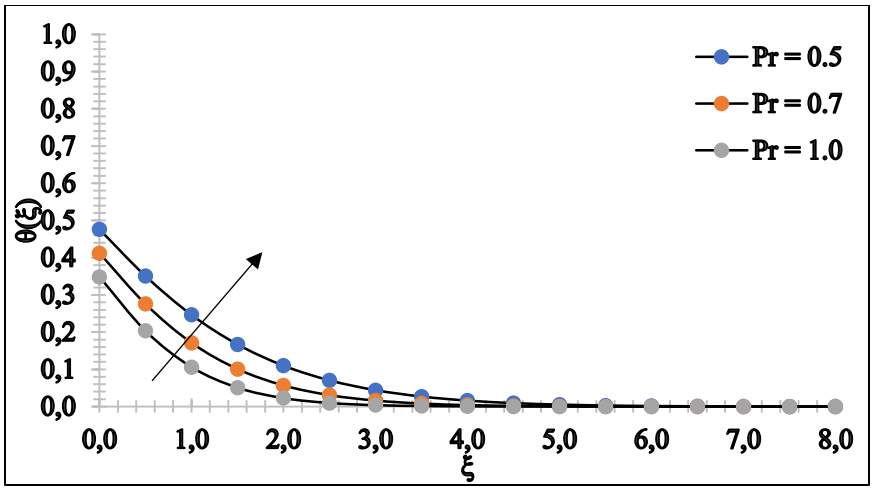

Figure 16: Influence of Pr on $\theta(\xi)$.

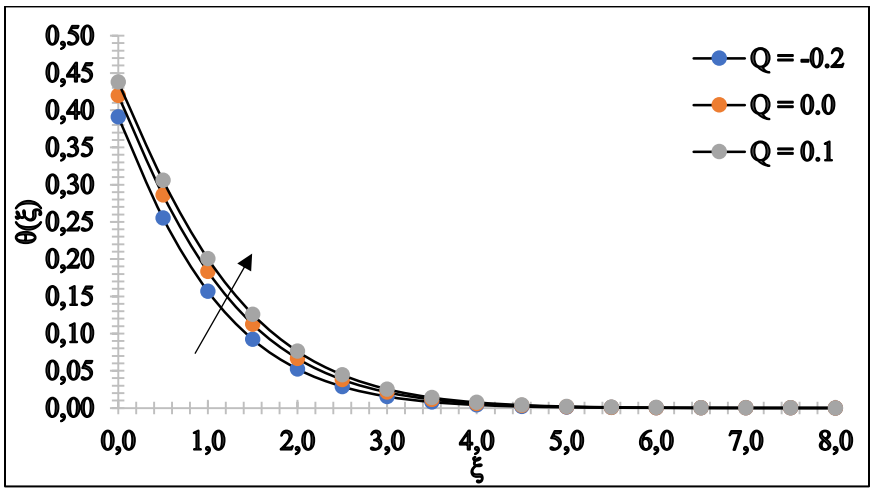

Figure 17: Influence of Q on $\theta(\xi)$.

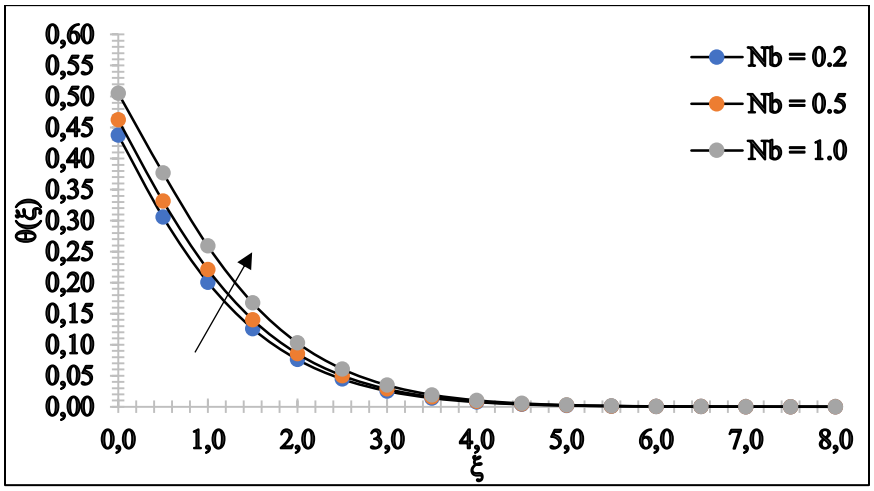

Figure 18: Influence of Nb on $\theta(\xi)$

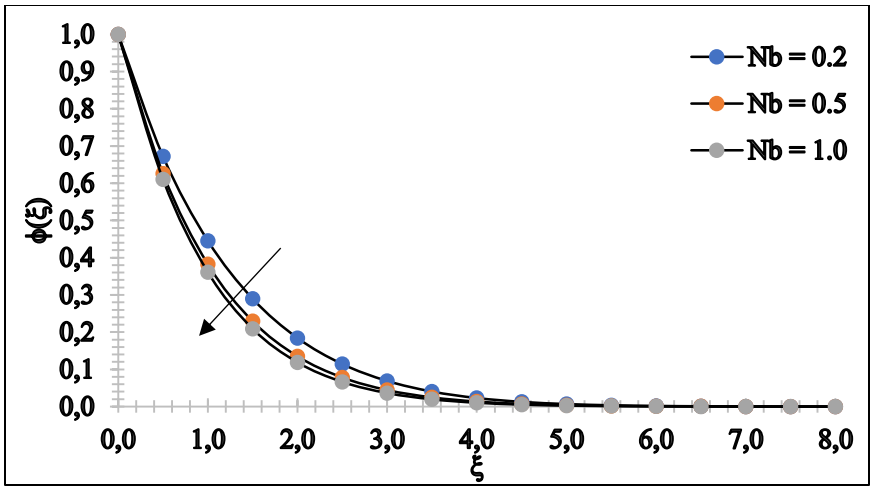

Figure 19: Influence of Nb on $\phi(\xi)$

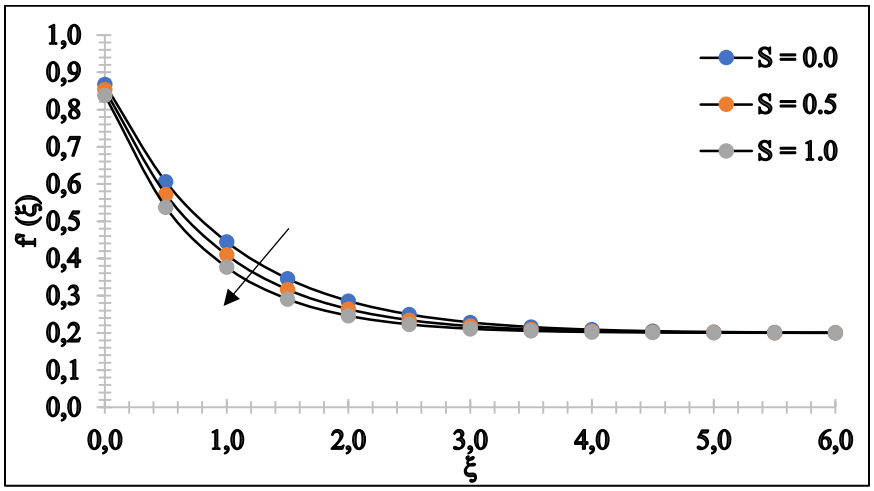

Figure 20: Influence of S on $f'(\xi)$.

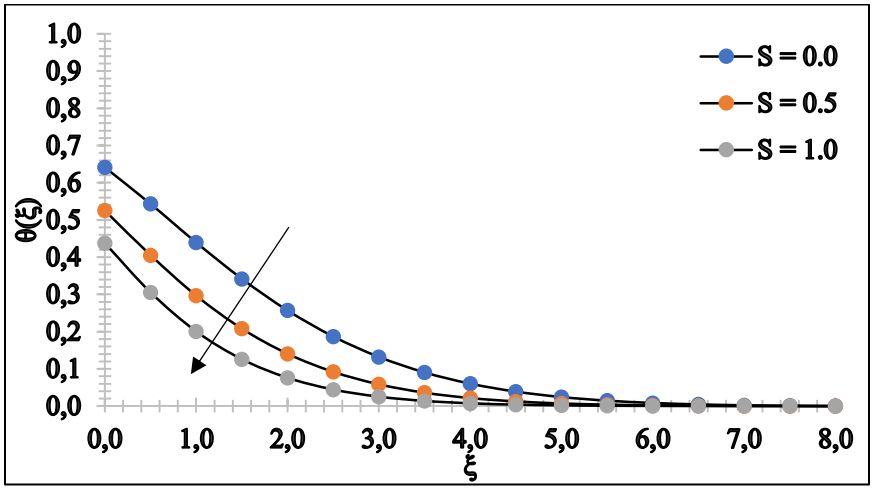

Figure 21: Influence of S on $\theta(\xi)$.

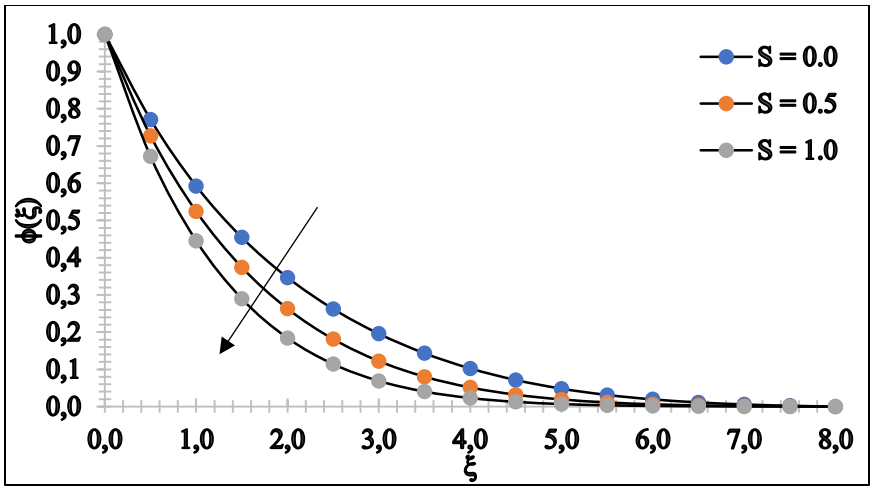

Figure 22: Influence of S on $\phi(\xi)$.

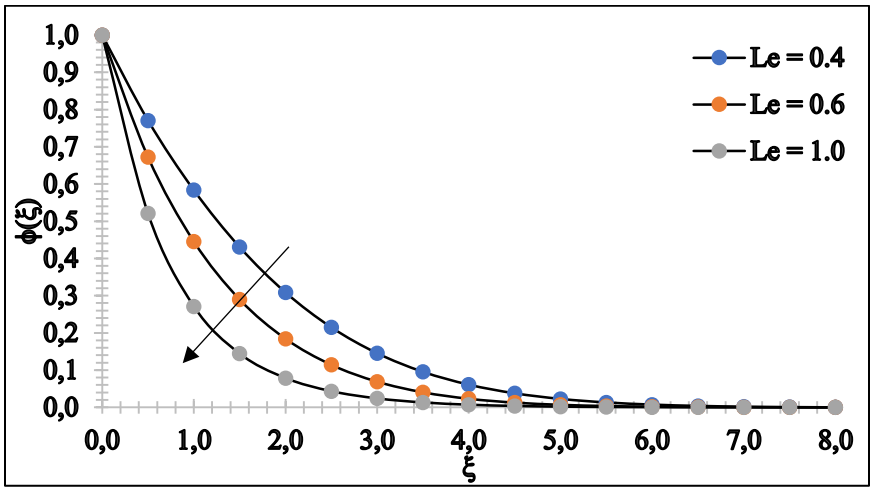

Figure 23: Influence of Le on $\phi(\xi)$

7. Conclusion

The overall conclusion drawn from the present work is summarized below.

- ❖ Decreasing behavior due to increasing the Casson fluid parameter in the velocity distribution and same behavior is noticed for enhancing the numerical value of suction parameter.
- ❖ For the large value of magnetic parameter, the velocity field reduce but opposite trend is observed in the graph of temperature and concentration distribution.
- ❖ The temperature distribution decelerate, and the concentration distribution accelerate due to boosting value of Prandtl number.
- ❖ Temperature profile rises by increasing radiation parameter and same behavior is observed in the temperature field because of thermophoresis parameter.
- ❖ Uprising of temperature field is observed for the increasing value of Eckert number.

Acknowledgements

Help by **Prf. S R Koneru**, Retd. Professor, Department of Mathematics, IIT Mumbai in the preparation of this paper is gratefully acknowledged.

Conflict of Interest

The authors declare no competing interests.

References

[1] Y. A. Cengel and J. M. Cimbala, Fluid mechanics: fundamentals and applications. McGraw-Hill, 1st edition, **2004**.

[2] B. Xia and D. W. Sun, Applications of computational fluid dynamics (CFD) in the food industry: review, Computers and electronics in agriculture, vol. 34, no. 1-3, pp. 5–24, **2002**.

[3] R. Banerjee, X. Bai, D. Pugh, K. Isaac, D. Klein, J. Edson, W. Breig, and L. Oliver, CFD simulations of critical components in fuel filling systems, SAE technical paper, Tech. Rep., **2002**.

[4] S. U. S. Choi, Nanofluid technology: current status and future research, Argonne national lab. (ANL), Argonne, IL (United States), Tech. Rep., **1998**.

[5] J. Buongiorno, Convective transport in nanofluids, Journal of heat transfer, vol. 128, no. 3, pp. 240–250, **2006**.

[6] S. Naramgari and C. Sulochana, MHD flow over a permeable stretching/shrinking sheet of a nanofluid with suction/injection, Alexandria engineering journal, vol. 55, no. 2, pp. 819–827, **2016**.

[7] M. H. Abolbashari, N. Freidoonimehr, F. Nazari, and M. M. Rashidi, Analytical modeling of entropy generation for Casson nanofluid flow induced by a stretching surface, Advanced powder technology, vol. 26, no. 2, pp. 542–552, **2015**.

[8] S. Ghadikolaei, K. Hosseinzadeh, D. Ganji, and B. Jafari, Nonlinear thermal radiation effect on magneto Casson nanofluid flow with Joule heating effect over an inclined porous stretching sheet, Case studies in thermal engineering, vol. 12, pp. 176–187, **2018**.

[9] H. M. Shawky, N. T. Eldabe, K. A. Kamel, and E. A. Abd-Aziz, MHD flow with heat and mass transfer of Williamson nanofluid over stretching sheet through porous medium, Microsystem technologies, vol. 25, no. 4, pp. 1155–1169, **2019**.

[10] M. E. Yazdi, A. Moradi, and S. Dinarvand, MHD mixed convection stagnation-point flow over a stretching vertical plate in porous medium filled with a nanofluid in the presence of thermal radiation, Arabian journal for science and engineering, vol. 39, no. 3, pp. 2251–2261, **2014**.

[11] K. A. Kumar, V. Sugunamma, N. Sandeep, and J. R. Reddy, MHD stagnation point flow of Williamson and Casson fluids past an extended cylinder: a new heat flux model, SN applied sciences, vol. 1, no. 7, pp. 705, **2019**.

[12] F. Aman, A. Ishak, and I. Pop, Magnetohydrodynamic stagnation-point flow towards a stretching/shrinking sheet with slip effects, International communications in heat and mass transfer, vol. 47, pp. 68–72, **2013**.

[13] H. Alfven, Existence of electromagnetic-hydrodynamic waves, Nature, vol.150, no. 3805, p. 405, **1942**.
[14] K. Hiemenz, The boundary layer on a straight circular cylinder immersed in the uniform liquid flow, J. Dinglers polytech, vol. 326, pp. 321–324, **1911**.
[15] E. Eckert, The calculation of the heat transfer in the laminar boundary layer around the body, VDI research issue, vol. 416, pp. 1–24, **1942**.
[16] T. R. Mahapatra and A. Gupta, Heat transfer in stagnation-point flow towards a stretching sheet," Heat and mass transfer, vol. 38, no. 6, pp. 517–521, **2002**.
[17] A. Ishak, R. Nazar, and I. Pop, Mixed convection boundary layers in the stagnation-point flow toward a stretching vertical sheet, Meccanica, vol. 41, no. 5, pp. 509–518, **2006**.
[18] T. Hayat, M. Mustafa, S. Shehzad, and S. Obaidat, Melting heat transfer in the stagnation-point flow of an upper convected Maxwell (UCM) fluid past a stretching sheet, International journal for numerical methods in fluids, vol. 68, no. 2, pp. 233–243, **2012**.
[19] T. Hayat, M. Awais, and M. Sajid, \Mass transfer effects on the unsteady flow of UCM fluid over a stretching sheet," International journal of modern physics, vol. 25, no. 21, pp. 2863–2878, **2011**.
[20] A. Jasmine Benazir, R. Sivaraj, and O. D. Makinde, Unsteady magnetohydrodynamic Casson fluid flow over a vertical cone and at plate with non-uniform heat source/sink, in international journal of engineering research in africa, vol. 21, Trans tech publ. Elsevier, pp. 69–83, **2016**.
[21] I. Animasaun, E. Adebile, and A. Fagbade, Casson fluid flow with variable thermo-physical property along exponentially stretching sheet with suction and exponentially decaying internal heat generation using the homotopy analysis method, Journal of the Nigerian mathematical society, vol. 35, no. 1, pp. 1–17, **2016**.
[22] M. Afikuzzaman, M. Ferdows, and M. M. Alam, Unsteady MHD Casson fluid flow through a parallel plate with hall current, Procedia engineering, vol. 105, pp. 287–293, **2015**.
[23] Kamatam Govardhan, Ganji Narender, Gobburu Sreedhar Sarma, Viscous dissipation and chemical reaction effects on MHD Casson nanofluid over a stretching sheet, Malaysian Journal of Fundamental and Applied Sciences, vol. 15, no. 4, pp. 585–592, **2019**.
[24] S. Ibrahim, P. Kumar, G. Lorenzini, E. Lorenzini, and F. Mabood, Numerical study of the onset of chemical reaction and heat source on dissipative MHD stagnation point flow of Casson nanofluid over a nonlinear stretching sheet with velocity slip and convective boundary conditions, Journal of engineering thermophysics, vol. 26, no. 2, pp. 256–271, **2017**.